Photoacoustic Imaging for Noninvasive Periodontal Probing Depth Measurements

Journal of Dental Research
2018, Vol. 97(1) 23–30

DOI: 10.1177/0022034517729820
journals.sagepub.com/home/jdr

C.Y. Lin[1], F. Chen[1,2], A. Hariri[1], C.J. Chen[1], P. Wilder-Smith[3], T. Takesh[3], and J.V. Jokerst[1,2,4]

Abstract

The periodontal probe is the gold standard tool for periodontal examinations, including probing depth measurements, but is limited by systematic and random errors. Here, we used photoacoustic ultrasound for high–spatial resolution imaging of probing depths. Specific contrast from dental pockets was achieved with food-grade cuttlefish ink as a contrast medium. Here, 39 porcine teeth (12 teeth with artificially deeper pockets) were treated with the contrast agent, and the probing depths were measured with novel photoacoustic imaging and a Williams periodontal probe. There were statistically significant differences between the 2 measurement approaches for distal, lingual, and buccal sites but not mesial. Bland-Altman analysis revealed that all bias values were < ±0.25 mm, and the coefficients of variation for 5 replicates were <11%. The photoacoustic imaging approach also offered 0.01-mm precision and could cover the entire pocket, as opposed to the probe-based approach, which is limited to only a few sites. This report is the first to use photoacoustic imaging for probing depth measurements with potential implications to the dental field, including tools for automated dental examinations or noninvasive examinations.

Keywords: periodontal exam, gingival thickness, ultrasound imaging, dental contrast agent, melanin nanoparticles, pocket depth

Introduction

The periodontal examination evaluates the periodontium for signs of inflammation or damage and is the basis for subsequent intervention. One key feature of this assessment is the measurement of probing depths—a numeric metric that reflects the extent of apical epithelial attachment relative to the gingival margin (Perry et al. 2014). Probing depth measurements can identify periodontal disease and monitor response to intervention. The probe depths offer insight into clinical attachment loss, furcation involvement, and bone loss when used in conjunction with radiography and the oral examination.

Probing depths are commonly measured with a periodontal probe, which have remained popular despite the advent of many next-generation tools (Hefti 1997). Unfortunately, probing depth measurements are error prone and suffer from poor reproducibility, largely due to variation in probing force. Indeed, a recent meta-analysis showed that a range of probing forces were used (51 to 995 N/cm^2)—a variation of ~20-fold (Larsen et al. 2009). Other error sources include variation in the insertion point, probe angulation, the patient's overall gingival health (weakly inflamed tissue), and the presence of calculus (Biddle et al. 2001; Perry et al. 2014). Thus, the examination is subject to large errors with interoperator variation as high as 40% and r values <0.80 (Listgarten 1980). These error sources can result in poor patient treatment and, hence, poor patient outcomes. This variation also compromises epidemiologic studies and makes it difficult to compare outcomes among dentists or among populations (Holtfreter et al. 2015). Furthermore, the probe often penetrates the inflamed epithelium, resulting in bleeding on probing (Lang et al. 1986; Lang et al. 1990) and producing probe depths that are up to 1 mm deeper than the actual anatomic value (Armitage et al. 1977; Perry et al. 2014). While some studies have shown that a constant force probe or digital probe might overcome most limitations, they underestimate probing with little improvement in reproducibility (Walsh and Saxby 1989). Clearly, new tools—including improved imaging tools—are urgently needed to improve this vital procedure.

Ultrasound is an affordable, high-resolution, sensitive, nonionizing, and real-time tool for imaging but is rarely used in dentistry. Previous studies have used ultrasound with frequencies ≤20 MHz to image facial crestal bone or the cementoenamel junction, but these approaches lacked the spatial resolution and contrast needed to measure probing depth (Nguyen et al. 2016; Chan et al. 2017). More recently, photoacoustic imaging has

[1]Department of NanoEngineering, University of California, San Diego, La Jolla, CA, USA
[2]Materials Science and Engineering Program, University of California, San Diego, La Jolla, CA, USA
[3]Beckman Laser Institute, University of California, Irvine, CA, USA
[4]Department of Radiology, University of California, San Diego, La Jolla, CA, USA

Corresponding Author:
J.V. Jokerst, Department of NanoEngineering, University of California, San Diego, 9500 Gilman Drive, La Jolla, CA 92092, USA.
Email: jjokerst@ucsd.edu

been used in addition to ultrasound to combine the temporal and spatial resolution of acoustics with the spectral behavior and increased contrast of optics (Ntziachristos and Razansky 2010; Wang and Hu 2012; Yin et al. 2017). In addition, the use of high frequency offers <100-μm resolution to image the probing depths. Here, for the first time, we used photoacoustic imaging in tandem with a food-grade oral rinse to estimate probing depths in a porcine model, and we compared the results with a gold standard periodontal probe. The results suggest that photoacoustic imaging could become a complementary tool for the dental community to image pockets and measure probe depth noninvasively.

Materials and Methods

Reagents

Cuttlefish ink A was from Conservas de Cambados, and ink B was from Nortindal. Both contained cuttlefish ink, water, salt, and sodium carboxymethyl cellulose as a thickener. Cornstarch was purchased from the local food store. Porcine heads were purchased from the local butcher—the Animal Ethic Committee does not regulate cadaver tissues. Agarose was purchased from Life Technologies. India ink solution 0.2% in phosphate-buffered saline (PBS) buffer was purchased from Thermo Fisher Scientific. Intralipid 20% and PBS tablets were purchased from Sigma-Aldrich. Polyethylene tubing (outside diameter: 1.27 mm, inside diameter: 0.85 mm) was purchased from Harvard Apparatus.

Equipment

Transmission electron microscopy (TEM) images were performed with a JEOL JEM-1200-EX II operating at 80 kV. The absorbance spectra were measured with a SpectraMax M5 spectrophotometer. The hydrodynamic radius was measured with a Zetasizer from Malvern via dynamic light scattering. The photoacoustic images were performed with a Vevo LAZR imaging system (Visualsonics) equipped with a 21 or 40 MHz–centered transducer as described previously (Ho et al. 2015; Wang et al. 2016).

Preparation of Cuttlefish Ink Derivatives

To measure the absorbance and photoacoustic spectra, 50% ink A (weight per volume) and 10% ink B (weight per volume) were prepared with 0.1M PBS solution, sonicated for 1 h, and further diluted. Ink A was diluted 50-fold and ink B, 10-fold, with 0.1M PBS solution to make a 1% solution. These samples were used for absorbance measurements; 1% solutions were made for photoacoustic spectral analysis. Corn starch (0.04 g) and ink A (0.04, 0.2, and 0.4 mL) were mixed in 0.1M PBS and boiled to prepare 2 mL of cornstarch-enhanced contrast agent. The pH of freshly prepared contrast agent with 2% cornstarch and 5% cuttlefish ink was 7.4. This was adjusted to pH 6.2, 6.6, 7.0, and 7.8 with 6N HCL and/or NaOH. Samples were placed in tubing for photoacoustic imaging.

Preparation of Cuttlefish Melanin Nanoparticles for TEM Imaging

A stock solution of ink A was diluted into 1% in Millipore water, sonicated for 1 h, and centrifuged at 5,000 g for 15 min (Chen et al. 2009). The supernatant was removed, and the pellet was resuspended in Millipore water. This was repeated 6 times, and the resulting pellet was suspended in pure ethanol for TEM imaging or PBS for dynamic light scattering.

Preparation of Tissue-Mimicking Phantom

The tissue-mimicking phantom was prepared with 0.5% (weight per volume [w/v]) ultrapure agarose solution, ~50% (volume per volume) india ink as the absorber, and 0.5% (w/v) Intralipid 20% as the scatter (Hanli et al. 1995; Nagarajan and Zhang 2011). These were prepared in 1% (w/v) ultrapure agarose. We used a custom phantom to measure penetration depth (Arconada-Alvarez et al. 2017).

Preparation of Porcine Jaw Samples

Frozen porcine heads were sliced sagittally with a band saw. The lower jaw was removed with a handsaw; soft tissues surrounding the jaw were dissected with a scalpel. Artificial deeper pockets were created with scalpels (Dynarex) to simulate periodontal lesions. The scalpel was applied parallel to the tooth with intrasulcular incisions until the scalpel contacted the bone (Weidmann et al. 2014). The contrast agent was pipetted onto the gingival line, and excess was rinsed with a syringe and 5 mL of deionized water. The jaw was immobilized in water for ultrasound coupling and imaged with a Vevo LAZR.

To test the signal stability, 1 molar of the mandible was rinsed 5 times with water after labeling. The jaw was imaged after each rinse to observe the photoacoustic signal. The tooth was then brushed for about 1 min without toothpaste after the final rinse. We then expanded this study to 13 molars. For each, the tooth was labeled, imaged, and brushed 5 times to calculate a coefficient of variation for the probing depth.

Periodontal Probing Depth Measurements

The probing depth was measured with a Williams probe following the direction of the tooth root (Mayfield et al. 1996) before photoacoustic imaging. The same examiner measured the periodontal probing depths with photoacoustic imaging and a Williams periodontal probe (Listgarten 1980). The Williams probe was marked at 1, 2, 3, 5, 7, 9, and 10 mm. In the maxilla, the probing depths were recorded at 4 sites per tooth: the mesial and distal sites of the tooth as well as 2 buccal locations below the anterior and posterior cusps of maxillary molar and fourth premolar. In the mandible, probing depths were recorded on the mesial and distal ends of the tooth as well as at 2 lingual locations below the anterior and posterior cusps of the mandibular molar (see Periodontal Labeling section).

Gingival Thickness Measurements

The gingival thickness values were measured with ultrasound imaging and compared with values collected with a needle and dental gauge analogous to methods with the UNC-15 and No. 25 K-file instruments (Vandana and Savitha 2005; Slak et al. 2015). Here, for each tooth, the measurement points were 2 mm below the gingival margin. A 28-gauge needle was then inserted perpendicularly into gingiva until it made contact with the tooth. We then drew a line on the needle where it made contact with the gingiva. After removal of the needle, the distance between the marked location and the tip of the needle was measured with dental gauge (0.1-mm precision).

Imaging Procedures

Typical imaging conditions included 100% laser energy; typical gains were 20 dB for photoacoustic and 10 dB for ultrasound. Photoacoustic spectra were collected from 680 to 970 nm. Porcine jaws were aligned parallel to the 40-MHz transducer and scanned from the crown to the root. The 3-dimensional scans were performed by oscillating between 680- and 800-nm excitation. All 3-dimensional images were processed as a maximum intensity projection.

Image Processing

Photoacoustic data were analyzed with ImageJ 1.48 (Abramoff et al. 2004). The intensity of each tube was measured in 8 regions of interest for statistical analysis. To discriminate the photoacoustic signal from stains and contrast agent, we collected data at both 680 and 800 nm. We subtracted the image at 680 nm from the one at 800 nm excitation. The resulting pixels were coded blue. These blue pixels were overlaid on the original image created with 680-nm excitation that had already been coded red. Only 680-nm excitation was used to image stain in the absence of contrast agent. The periodontal probing depths were measured on the sagittal view of 3-dimensional images with the Vevo LAB software.

Statistical Treatment

The mean, standard deviation, Bland-Altman plots, and coefficient of variation (CV) were based on GraphPad Prism 5 (Bland and Altman 1986). All error bars represent the standard deviation. Here, $P < 0.05$ was considered significant.

Results

Characterization of Cuttlefish Ink Derivatives

TEM (Fig. 1A) showed that the cuttlefish ink contained spherical melanin nanoparticles (Ju et al. 2013); the measurement of 500 nanoparticles via TEM indicated a mean size of 125.1 nm (Fig. 1B). Dynamic light scattering showed that the mean size was 266.3 nm with a polydispersity index of 0.116 (i.e., a measure of size uniformity; <0.3 indicates uniformity). Both inks had a broad photoacoustic spectrum from 680 to 970 nm; ink A had 2-fold-stronger signal intensity than ink B at 680 nm (both at 1%; Fig. 1C). Thus, ink A was used for all subsequent experiments.

Figure 1D shows the photoacoustic (red) and ultrasound (black and white) mode images of the ink/cornstarch contrast agent at different concentrations. The photoacoustic signal increased proportionally to ink concentration ($R^2 = 0.96$); 2% cornstarch alone had no photoacoustic signal. We also evaluated the effect of pH on photoacoustic signal but saw no significant change from pH 6.2 to 7.8 (Fig. 1E). The photoacoustic signal of the contrast agent as a function of depth in tissue phantom was quantified (Fig. 1F) and showed that 1-cm imaging was routine.

Periodontal Labeling

Next, we measured the probing depth with imaging and a Williams probe (Fig. 2A) at mesial, distal, lingual, and buccal locations. Imaging was complicated by endogenous stains on the porcine teeth (Fig. 2B). Fortunately, the contrast agents had similar signal at 800 and 680 nm, but the signal of the stains decreased about 50% at 800 nm relative to 680 nm (Fig. 2C). Thus, we used photoacoustic spectroscopy to discriminate between stained teeth (Fig. 2D) and the signal of the contrast agent (Fig. 2E).

Figure 2G shows combined ultrasound and photoacoustic images in a sagittal view of the tooth. Hard and soft dental tissues were obvious. The photoacoustic signal in the pocket started from the gingival margin and extended along the root. We also evaluated the stability with additional water rinses, but the signal did not decrease (<0.2% after 5 washes). This was repeated at the mesial, lingual, and distal locations, including up to 5 rinse cycles, but no significant decrease was seen ($P > 0.05$). Fortunately, the contrast agent was easily removed via teeth brushing.

Periodontal Probing Depth Measurements

Figure 3A shows shallow, intermediate, and deep pockets and artificially created deep pockets. We created the artificially deep pockets because swine have shallow pockets, but evaluating the technique in deep pockets was a key goal. Figure 3B–D compares the periodontal probing depths measured by photoacoustic imaging with depths measured with a probe at mesial ($n = 39$), lingual and buccal ($n = 78$), and distal ($n = 39$) locations. We combined the lingual and buccal groups because of their similar geometry.

We compared photoacoustic data with Williams probe data via a paired t test. There was no significant difference for the mesial data, but the distal and lingual/buccal groups were significantly different ($P < 0.05$). The distal and mesial pockets were underestimated by photoacoustics, but the lingual and buccal sites were overestimated with photoacoustics relative to periodontal probe. We also divided the combined lingual/

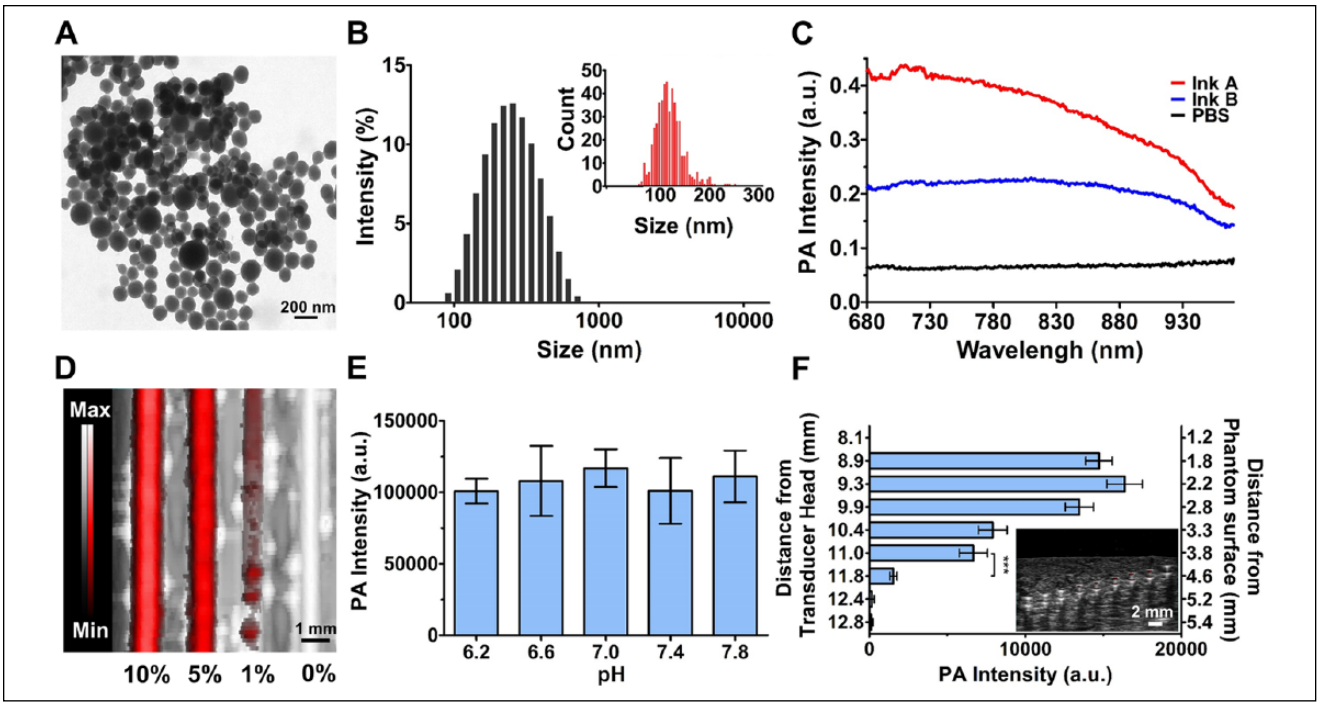

Figure 1. Characterization of cuttlefish ink and photoacoustic signal of cuttlefish ink/cornstarch contrast agent. (**A**) Transmission electron microscopy image of 0.5% ink A illustrating the spherical melanin nanoparticles found in cuttlefish ink. (**B**) The hydrodynamic radius of melanin nanoparticles in phosphate buffered saline (PBS) by dynamic light scattering was 266.3 nm, with a polydispersity index of 0.116; the insert figure is the measurement of 500 nanoparticles on transmission electron microscopy images, indicating a mean size of 125.1 nm. (**C**) Photoacoustic spectra of inks A and B were studied at 1% in 0.1M PBS. (**D**) Overlaid ultrasound mode (grayscale) and photoacoustic (red) images of a phantom with cuttlefish ink/cornstarch contrast agent with 2% cornstarch and 10%, 5%, 1%, ad 0% cuttlefish ink. (**E**) Imaging data as a function of pH show that the photoacoustic signal of the contrast agent with 5% cuttlefish ink and 2% cornstarch was stable from pH 6.2 to 7.8. (**F**) Photoacoustic intensity as a function of depth was performed for a cuttlefish ink/cornstarch contrast agent with 5% cuttlefish ink and 2% cornstarch, except for the uppermost sample (PBS control). The signal 11 mm from the transducer head was >4-fold higher than that at 11.8 mm. For panels E and F, the error bars represent the standard deviation of 8 regions of interest. ***$P < 0.0001$ (unpaired Student's t test).

buccal groups into lingual only and buccal only. These also showed a significant difference ($P < 0.05$). Thus, we further quantified these data via Bland-Altman analysis.

Bland-Altman plots show that 95% of the samples fell within 1.96 standard deviations of the differences between the 2 methods (95% confidence interval [95% CI]) at mesial, lingual and buccal, and distal locations (Fig. 4). Small bias values of −0.18, 0.08, and −0.21 mm were identified at mesial, lingual and buccal, and distal locations, respectively; the 95% CIs are plotted as well and are all <1.0 mm, except at mesial locations (Fig. 4). Thus, the photoacoustic measurements were slightly lower, higher, and lower at mesial, lingual and buccal, and distal locations, respectively. We repeated Bland-Altman analysis separately for lingual and buccal sites. Buccal ($n = 56$) sites had a bias of 0.05 mm (95% CI, 0.81 to −0.72 mm); lingual ($n = 22$) sites had a bias of 0.20 mm (95% CI, 0.84 to −0.44 mm).

We conducted additional experiments to more carefully evaluate consistency of probing (Fig. 4D). We studied 13 teeth over 5 replicates. At each replicate, we measured the mesial, distal, and lingual/buccal locations. The CV for the 5 replicates were all <11%. The raw values for the CV are plotted in Figure 4D for all 13 teeth. The mean CV values were ~6%.

Gingival Thickness Measurement

Figure 5A shows that the gingival thickness can also be precisely measured via the ultrasound-mode data with a high-frequency ultrasound transducer (40 MHz). The gingival thickness measured with ultrasound imaging and with a needle for 45 teeth is 1.40 ± 0.25 mm and 1.33 ± 0.28 mm, respectively. The Bland-Altman plot (Fig. 5B) shows that the bias was 0.07 mm, indicating that needle measurements gave slightly lower values.

Discussion

This study reports photoacoustic imaging with the melanin nanoparticles in cuttlefish ink as a contrast agent for noninvasive measurements of probing depths. Melanin has broad optical absorption for photoacoustic imaging (Viator et al. 2004). It is a common foodstuff with no safety concerns (Chaitanya 2014). The pH of saliva can range from 6.2 to 7.4 (Schipper et al. 2007), but this contrast agent has good signal stability regardless of pH (Fig. 1C).

Porcine teeth often have yellow-brown stains with background photoacoustic signal, but this could be spectrally

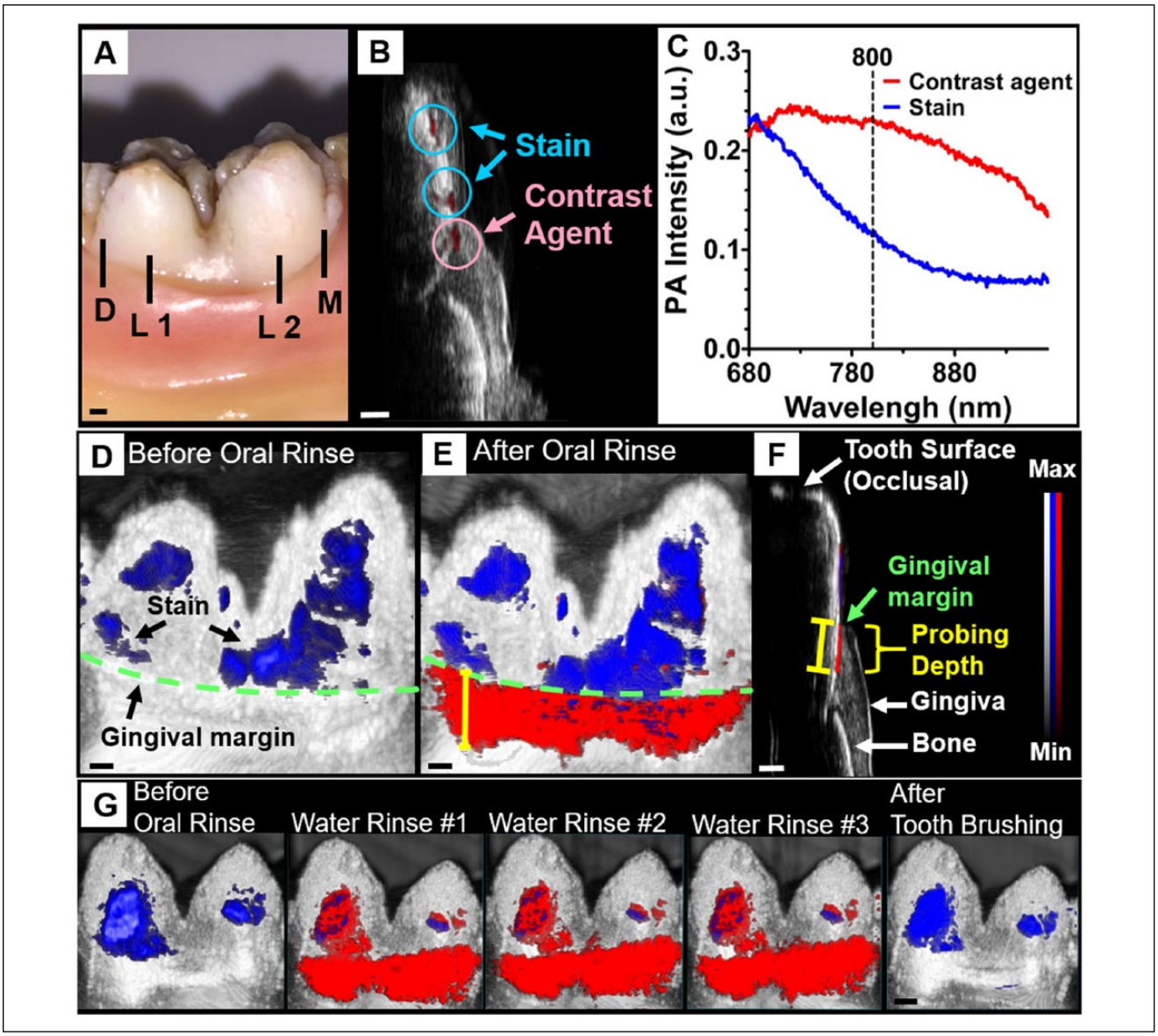

Figure 2. Representative images of periodontal probing depth measurement. (**A**) Illustration of distal, lingual, and mesial probing locations in the porcine tooth. (**B**) The photoacoustic image from a tooth with stains and a contrast agent with 680-nm excitation. (**C**) The contrast agent and stain had a similar signal at 680 nm, but the signal of the stain decreased about 50% at 800 nm. This was used to discriminate between the 2 absorbers. Photoacoustic/ultrasound images before (**D**) and after (**E**) cuttlefish ink/cornstarch contrast agent treatment. The blue color is a photoacoustic signal from stains on the teeth, and the red color is photoacoustic signal from a cuttlefish ink/cornstarch contrast agent. The green dashed line is the gingival margin, and the yellow bar represents the probing depth. (**F**) This sagittal view of a 3-dimensional scan on a tooth clearly illustrates both hard and soft dental tissues, and the photoacoustic signal of the contrast agent in the pocket started from the gingival margin and extended along the root direction analogous to a probing depth measurement. This sagittal view shows the tooth surface, gingival margin, gingiva, and bone; the probing depth is obvious when the tooth is viewed in a sagittal plane after contrast agent treatment. (**G**) Photoacoustic/ultrasound images acquired before and after ink treatment, followed by multiple water rinses. The contrast agent remained in the pocket for 5 rinses (only 3 shown here for economy of space). The contrast agent was easily removed after brushing. The scale bars are 1 mm.

discriminated from the squid ink contrast agent (Fig. 2B). Spectral imaging may have utility in future applications, including the use of multiple contrast agents concurrently for applications in mineralization or biofilm characterization.

One other issue with porcine models is the small probing depths relative to human subjects (2 to 3 mm, healthy; 4 to 5 mm with gingivitis; Wang et al. 2007). Most pockets were <3 mm, and only ~10% of teeth had pockets >3 mm; thus, we created 12 deeper pockets and repeated the imaging and depth measurements. These are shown as squares in Figure 3. These artificial pockets also correlated to the Williams probe. We included these data points in the Bland-Altman analysis in Figure 4 but noted only minor changes (bias of −0.04 to −0.18 mm for mesial, 0.17 to 0.08 mm for lingual/buccal, and −0.20 to −21 mm for distal locations).

Despite these challenges, photoacoustic imaging offers much more precise and continuous data on probing depths. In the clinic, probing depths are recorded at only 6 sites per tooth.

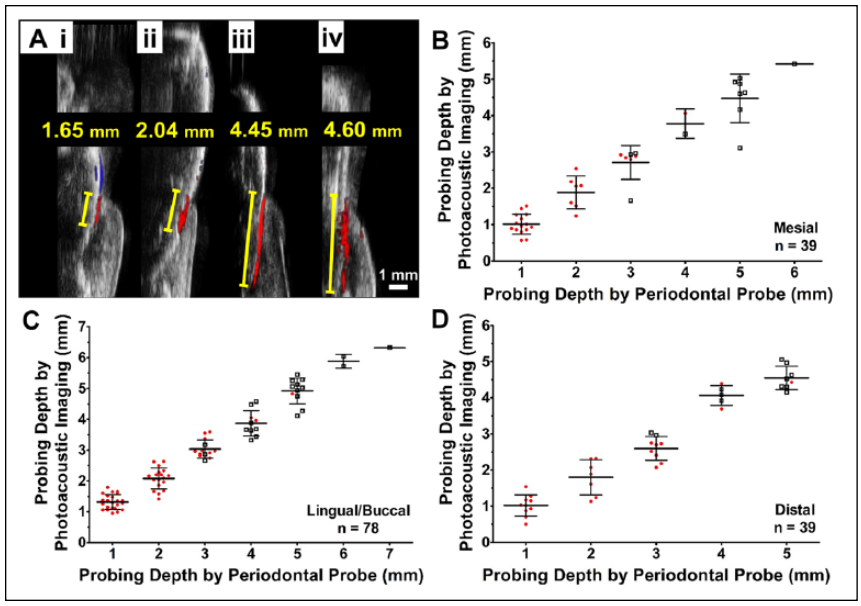

Figure 3. Periodontal probing depth measurements and comparison between methods. (**A**) Representative images, including shallow (1.65 mm; i), intermediate (2.04 mm; ii), deep (4.45 mm; iii), and artificially deep (4.60 mm; iv) pockets obtained via photoacoustic imaging. Comparisons of probing depth measured by periodontal probe and by imaging at (**B**) mesial, (**C**) lingual and buccal, and (**D**) distal locations of molars. The blue circles and hollow squares are the results of natural and artificial pockets, respectively. The bars indicate the mean probing depth measured by photoacoustic imaging. The error bars represent the standard deviation of the depths measured by photoacoustic imaging.

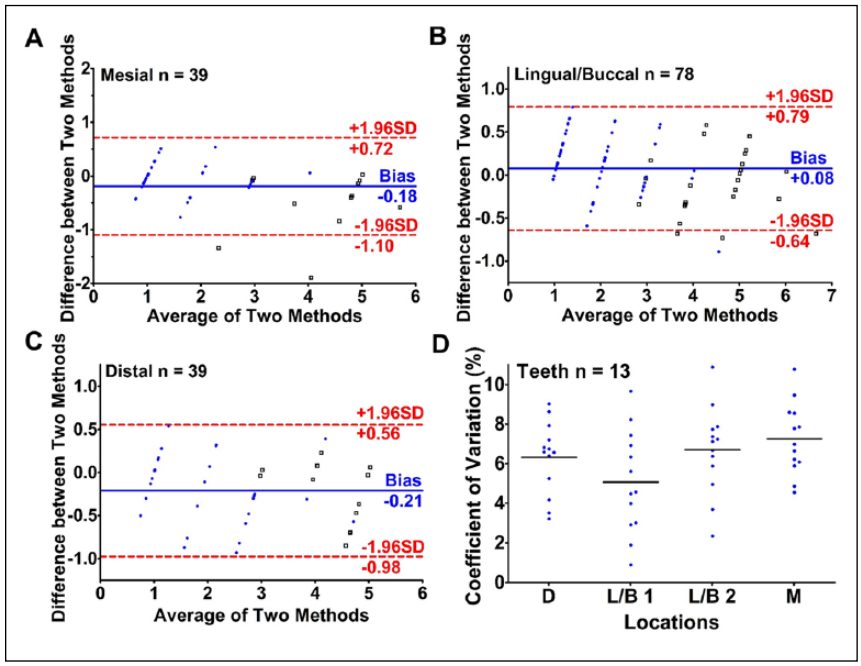

Figure 4. Bland-Altman plots. Comparison of agreement between probing depths measured by photoacoustic imaging and Williams probe at (**A**) mesial, (**B**) lingual and buccal, and (**C**) distal locations of molars. The blue circles and hollow squares are the results of natural and artificial pockets, respectively. The bias values were calculated by subtracting the depth measured by photoacoustic imaging by the depth measured with the Williams probe. (**D**) The coefficient of variation for the 5 replicates in mesial, lingual/buccal, and distal locations were all <11% for all 13 teeth. The mean coefficient of variation values were ~6%.

Figure 3B–D show that this imaging approach can measure the probing depths at all points along the tooth. This can markedly minimize sampling error, and it might be able to detect isolated deeper pockets that may be indicative of vertical root fractures (Khasnis et al. 2014). This imaging approach also eliminates variation in the probe insertion point and angle (Murphy et al. 2012) and could eliminate the error results from the presence of calculus.

The spatial resolution of the 40-MHz transducer is 100 μm by ultrasound and approximately 300 μm in photoacoustic mode. Thus, this approach offers more precision among different depths as opposed to the Williams probe, which rounds to the nearest millimeter. This may have utility in monitoring/predicting therapy where small changes can have significant implications (Fiorellini 2016). The photoacoustic approach had a positive bias in lingual and buccal locations perhaps because they were more easily aligned beneath the transducer (Fig. 4); mesial and distal sites are slightly more difficult to access with the transducer.

Figure 5B shows that the thicknesses measured on ultrasound mode images were 0.07 mm larger than invasive examinations. Gold standard methods include the UNC-15 and No. 25 K-file instruments (Vandana and Savitha 2005; Slak et al. 2015), but these are quite painful and require anesthesia. Other studies have shown that the mean thicknesses measured with A-line ultrasound were slightly higher than the invasive method perhaps because of the pressure placed on the gingiva during a physical examination (Vandana and Savitha 2005; Slak et al. 2015).

This study has some limitations. First, the optical excitation and acoustic pressure waves can be absorbed and scattered by bone. Thus, this technique might have limited utility with infrabony pockets as well as with interproximal pockets. Second, restorations might generate background interfering photoacoustic signal, but this could be gated out spectrally as with the aforementioned stains (Balderas-López et al. 1999). Third, pressure of crevicular fluid in the pockets has been shown to cause incomplete penetration of local irrigations into the

full depth of pockets (Fjærtoft et al. 1992). This might limit the depth with which the squid ink–based contrast could enter the pockets. Fourth, the porcine model had relatively shallow pockets that might not accurately represent human disease. While we created artificially deeper pockets, these may not truly mimic human disease.

There are limited reports of photoacoustics in dentistry, including implant characterization (Lee et al. 2017) and caries identification (Cheng et al. 2016). Smaller LED-based systems have recently been created with logarithmic reductions in cost and complexity. These innovations will likely make photoacoustic imaging more accessible to the dental community.

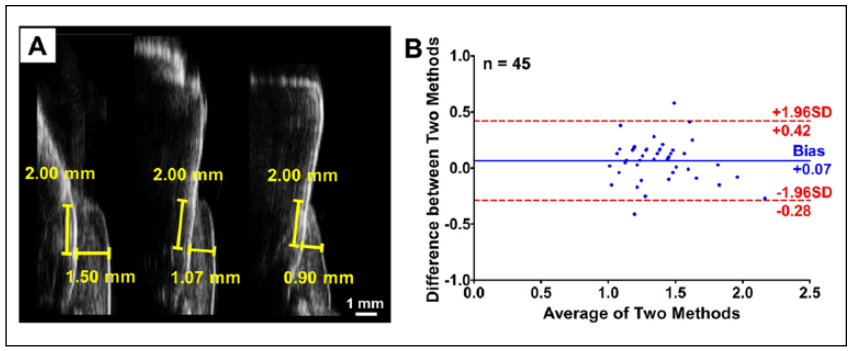

Figure 5. Gingival thickness measurement. (**A**) Representative ultrasound mode images showing the precise measurements obtained with a 40-MHz ultrasound transducer. (**B**) Comparison of agreement between gingival thicknesses measured by ultrasound imaging and by needle 2 mm from the gingival margin. The difference was calculated by the thicknesses measured by ultrasound minus the value obtained with a needle.

Conclusion

This study demonstrated for the first time that probing depths could be measured with photoacoustic imaging. The values that we achieved with this novel technique agreed nicely with the gold standard periodontal probe approach but were more precise, offered higher resolution images, and covered all areas of the tooth. The gingival thickness could also be easily measured. Future work will use models of periodontal disease as well as automated algorithms to collect and process the data.

Author Contributions

C.Y. Lin, J.V. Jokerst, contributed to conception, design, data acquisition, analysis, and interpretation, drafted and critically revised the manuscript; F. Chen, A. Hariri, C.J. Chen, P. Wilder-Smith, T. Takesh, contributed to data acquisition, critically revised the manuscript. All authors gave final approval and agree to be accountable for all aspects of the work.

Acknowledgments

We acknowledge the National Institutes of Health (grants DP2 HL137187 and S10 OD021821). We acknowledge Dr. Lem Moyé for statistical advice. The authors declare no potential conflicts of interest with respect to the authorship and/or publication of this article.

References

Abramoff MD, Magelhaes PJ, Ram SJ. 2004. Image processing with ImageJ. Biophotonics Int. 11(7):36–42.

Arconada-Alvarez SJ, Lemaster JE, Wang J, Jokerst JV. 2017. The development and characterization of a novel yet simple 3D printed tool to facilitate phantom imaging of photoacoustic contrast agents. Photoacoustics. 5:17–24.

Armitage GC, Svanberg GK, Loe H. 1977. Microscopic evaluation of clinical measurements of connective tissue attachment levels. J Clin Periodontol. 4(3):173–190.

Balderas-López JA, Moreno-Márquez MM, Martínez JL, Sánchez-Sinencio F. 1999. Thermal characterization of some dental resins using the photoacoustic phase lag discontinuities. Superficies y Vacio. 8:42–45.

Biddle AJ, Palmer RM, Wilson RF, Watts TL. 2001. Comparison of the validity of periodontal probing measurements in smokers and non-smokers. J Clin Periodontol. 28(8):806–812.

Bland JM, Altman DG. 1986. Statistical methods for assessing agreement between two methods of clinical measurement. Lancet. 1(8476):307–310.

Chaitanya L. 2014. Food coloring: the natural way. Res J Chem Sci. 4(2): 87–96.

Chan H-L, Sinjab K, Chung M-P, Chiang Y-C, Wang H-L, Giannobile WV, Kripfgans OD. 2017. Non-invasive evaluation of facial crestal bone with ultrasonography. PLoS One. 12(2):e0171237.

Chen S, Xue C, Wang J, Feng H, Wang Y, Ma Q, Wang D. 2009. Adsorption of Pb(II) and Cd(II) by squid *Ommastrephes bartrami* melanin. Bioinorg Chem Appl. 7:901563.

Cheng R, Shao J, Gao X, Tao C, Ge J, Liu X. 2016. Noninvasive assessment of early dental lesion using a dual-contrast photoacoustic tomography. Sci Rep. 6:21798.

Fiorellini JP. 2016. A classification system for peri-implant diseases and conditions. Int J Periodontics Restorative Dent. 36(5):699–705.

Fjærtoft M, Johannessen AC, Heyeraas KJ. 1992. Micropuncture measurements of interstitial fluid pressure in normal and inflamed gingiva in rats. J Periodontal Res. 27(5):534–538.

Hanli L, Boas DA, Yutao Z, Yodh AG, Chance B. 1995. Determination of optical properties and blood oxygenation in tissue using continuous NIR light. Phys Med Biol. 40(11):1983–1993.

Hefti AF. 1997. Periodontal probing. Crit Rev Oral Biol Med. 8(3):336–356.

Ho IT, Sessler JL, Gambhir SS, Jokerst JV. 2015. Parts per billion detection of uranium with a porphyrinoid-containing nanoparticle and in vivo photoacoustic imaging. Analyst. 140(11):3731–3737.

Holtfreter B, Albandar JM, Dietrich T, Dye BA, Eaton KA, Eke PI, Papapanou PN, Kocher T; Joint EU/USA Periodontal Epidemiology Working Group. 2015. Standards for reporting chronic periodontitis prevalence and severity in epidemiologic studies: proposed standards from the joint eu/USA periodontal epidemiology working group. J Clin Periodontol. 42(5):407–412.

Ju K-Y, Lee JW, Im GH, Lee S, Pyo J, Park SB, Lee JH, Lee J-K. 2013. Bio-inspired, melanin-like nanoparticles as a highly efficient contrast agent for T1-weighted magnetic resonance imaging. Biomacromolecules. 14(10):3491–3497.

Khasnis SA, Kidiyoor KH, Patil AB, Kenganal SB. 2014. Vertical root fractures and their management. J Conserv Dent. 17(2):103–110.

Lang NP, Adler R, Joss A, Nyman S. 1990. Absence of bleeding on probing: an indicator of periodontal stability. J Clin Periodontol. 17(10):714–721.

Lang NP, Joss A, Orsanic T, Gusberti FA, Siegrist BE. 1986. Bleeding on probing: a predictor for the progression of periodontal disease? J Clin Periodontol. 13(6):590–596.

Larsen C, Barendregt DS, Slot DE, Van der Velden U, Van der Weijden F. 2009. Probing pressure, a highly undervalued unit of measure in periodontal probing: a systematic review on its effect on probing pocket depth. J Clin Periodontol. 36(4):315–322.

Lee D, Park S, Noh W-C, Im J-S, Kim C. 2017. Photoacoustic imaging of dental implants in a porcine jawbone ex vivo. Opt Lett. 42(9):1760–1763.

Listgarten MA. 1980. Periodontal probing: what does it mean? J Clin Periodontol. 7(3):165–176.

Mayfield L, Bratthall G, Attstrom R. 1996. Periodontal probe precision using 4 different periodontal probes. J Clin Periodontol. 23(2):76–82.

Murphy NC, Bissada NF, Davidovitch Ze, Kucska S. 2012. Corticotomy and stem cell therapy for orthodontists and periodontists: rationale, hypotheses,

and protocol. In: Krishnan V, Davidovitch Z, editors. Integrated clinical orthodontics. Hoboken (NJ): John Wiley & Sons, Ltd. p. 392–421.
Nagarajan S, Zhang Y. 2011. Upconversion fluorescent nanoparticles as a potential tool for in-depth imaging. Nanotechnology. 22(39):395101.
Nguyen K-CT, Le LH, Kaipatur NR, Major PW. 2016. Imaging the cemento-enamel junction using a 20-mhz ultrasonic transducer. Ultrasound Med Biol. 42(1):333–338.
Ntziachristos V, Razansky D. 2010. Molecular imaging by means of multispectral optoacoustic tomography (MSOT). Chem Rev. 110(5):2783–2794.
Perry DA, Beemsterboer P, Essex G. 2014. Periodontology for the dental hygienist. St. Louis (MO): Elsevier/Saunders.
Schipper RG, Silletti E, Vingerhoeds MH. 2007. Saliva as research material: biochemical, physicochemical and practical aspects. Arch Oral Biol. 52(12):1114–1135.
Slak B, Daabous A, Bednarz W, Strumban E, Maev RG. 2015. Assessment of gingival thickness using an ultrasonic dental system prototype: a comparison to traditional methods. Ann Anat. 199:98–103.
Vandana KL, Savitha B. 2005. Thickness of gingiva in association with age, gender and dental arch location. J Clin Periodontol. 32(7):828–830.
Viator JA, Komadina J, Svaasand LO, Aguilar G, Choi B, Stuart Nelson J. 2004. A comparative study of photoacoustic and reflectance methods for determination of epidermal melanin content. J Invest Dermatol. 122(6):1432–1439.
Walsh TF, Saxby MS. 1989. Inter- and intra-examiner variability using standard and constant force periodontal probes. J Clin Periodontol. 16(3):140–143.
Wang J, Chen F, Arconada-Alvarez SJ, Hartanto J, Yap L-P, Park R, Wang F, Vorobyova I, Dagliyan G, Conti PS. 2016. A nanoscale tool for photoacoustic-based measurements of clotting time and therapeutic drug monitoring of heparin. Nano Lett. 16(10):6265–6271.
Wang LV, Hu S. 2012. Photoacoustic tomography: in vivo imaging from organelles to organs. Science. 335(6075):1458–1462.
Wang S, Liu Y, Fang D, Shi S. 2007. The miniature pig: a useful large animal model for dental and orofacial research. Oral Dis. 13(6):530–537.
Weidmann B, Sahrmann P, Bindl A, Roos M, Schmidlin PR. 2014. Depth determination of artificial periodontal pockets using cone-beam tomography and radio-opaque material: an in vitro feasibility study. Swiss Dent J. 124(4):406–415.
Yin C, Zhen X, Fan Q, Huang W, Pu K. 2017. Degradable semiconducting oligomer amphiphile for ratiometric photoacoustic imaging of hypochlorite. ACS Nano. 11(4):4174–4182.